

## Magnetic hyperbolic metamaterial of high-index nanowires

M. S. Mirmoosa,<sup>1</sup> S. Yu. Kosulnikov,<sup>1,2</sup> and C. R. Simovski<sup>1,2</sup>

<sup>1</sup>*Department of Radio Science and Engineering, School of Electrical Engineering, Aalto University, P.O. Box 13000, FI-00076 AALTO, Finland*

<sup>2</sup>*Department of Nanophotonics and Metamaterials, ITMO University, 197043 St. Petersburg, Russia*  
(Received 12 May 2016; revised manuscript received 11 July 2016; published 17 August 2016)

We show that the axial component of the magnetic permeability tensor is resonant for a wire medium consisting of high-index epsilon-positive nanowires, and its real part changes the sign at a certain frequency. At this frequency the medium experiences the topological phase transition between the elliptic and hyperbolic type of dispersion. We show that the transition regime is characterized by an extremely strong dependence of the permeability on the wave vector. This implies very high density of electromagnetic states that results in the filamentary pattern and noticeable Purcell factor for a transversely oriented magnetic dipole.

DOI: [10.1103/PhysRevB.94.075138](https://doi.org/10.1103/PhysRevB.94.075138)

### I. INTRODUCTION

Simple wire media, defined as optically dense arrays of parallel metal wires in a host dielectric material, have been getting considerable attention since electromagnetic metamaterials were introduced. Many applications of such media have been suggested from radio frequencies where the period of wire media is on the millimeter scale to optical frequencies where this period is submicron. Among them one can mention biological sensing [1], subwavelength imaging and endoscopy with image magnification [2–4], enhancement of quantum emitters, thermal sources, and classical dipole radiators [5–7], enhancement of radiative heat transfer [8–10], etc. More details can be found in Ref. [11]. In all these works, electromagnetic properties of wire media were described in a condensed form via an effective permittivity tensor:

$$\bar{\epsilon} = \begin{pmatrix} \epsilon_{\perp} & 0 & 0 \\ 0 & \epsilon_{\perp} & 0 \\ 0 & 0 & \epsilon_{\parallel} \end{pmatrix}. \quad (1)$$

Here,  $\epsilon_{\perp}$  and  $\epsilon_{\parallel}$  are the perpendicular (transversal) and parallel (axial) components with respect to the axis of the wires. Therefore, standard wire media are uniaxially anisotropic materials (though not usual ones because they possess spatial dispersion—dependence of  $\bar{\epsilon}$  on the wave vector  $\mathbf{k}$  [12,13]).

At infrared frequencies, the relative dielectric constant of the metal nanowires is highly negative. If the fraction ratio of the metal in the effective medium is low, the perpendicular component  $\epsilon_{\perp}$  of the permittivity is approximately equal to the permittivity of the host medium, whereas the parallel component  $\epsilon_{\parallel}$  has a negative sign [11,12]. For the dispersion, it implies that the transverse magnetic (TM) polarized wave has an open dispersion surface similar to a hyperboloid [11,13]. This dispersion surface results in the high density of electromagnetic states and enhancement of a subwavelength electric dipole located in the medium orthogonally to the wires [5,13]. The radiation of a magnetic dipole can also be enhanced, but this effect is lower because the dipole produces mainly TE waves whose electric field is orthogonal to nanowires. These transversely electric (TE) polarized waves weakly interact with the wire medium, and their dispersion surfaces are rather similar to spheres like dispersion

surfaces of free space. Notice that for metal nanowires the effective permeability tensor ( $\bar{\mu}$ ) is practically equal to unity [11].

Recently, in Ref. [14] one studied an anisotropic medium with artificial magnetism. This medium is dual to the dielectric hyperbolic metamaterial described by the indefinite tensor in Eq. (1). In this magnetic metamaterial the effective permeability tensor is not unity, and the dispersion surfaces of TE-polarized waves are hyperbolic and elliptic. However, the medium in Ref. [14] is not a wire medium. It is a racemic array of metal helices with both left-handedness and right-handedness. Such media, in accordance to initial works [15,16] where they were introduced, should be referred to as spiral media. The spiral medium of Ref. [14] operates at microwave frequencies, where metals are close to perfect conductors. In the present paper, we study wire media at optical frequencies. It is worth noting that at these frequencies, magnetic hyperbolic media have been recently observed experimentally. These media are called multilayer fishnet metamaterials [17].

Below, we theoretically demonstrate that a simple wire medium (see Fig. 1) may have in the infrared range similar electromagnetic properties to those manifested by Ref. [14] exhibited at microwaves, however, there are also significant peculiarities which share our wire medium out from all hyperbolic metamaterials. Nanowires of our wire medium should be made of high-index epsilon-positive materials such as lithium tantalate, silicon carbide, hexagonal boron nitride, or some other polaritonic materials (polaritonic rods have been used at THz and infrared frequencies to form effective bulk uniaxial media [6,18,19]. However, to the best of our knowledge, only the electric properties of these media have been considered). The resonance of the axial component of the effective permeability tensor arises because the dynamic magnetic polarizability of the high-index dielectric wire is resonant and originates from the Mie resonance of a single nanowire. We show that this axial permeability changes its sign at a certain frequency and in a narrow frequency range around this transition is a very sharp function of the wave vector. According to Ref. [20], this transition is called topological phase transition since the dispersion surface of the medium transits from the closed surface (elliptical regime) to open surface (hyperbolic regime). The corresponding topological

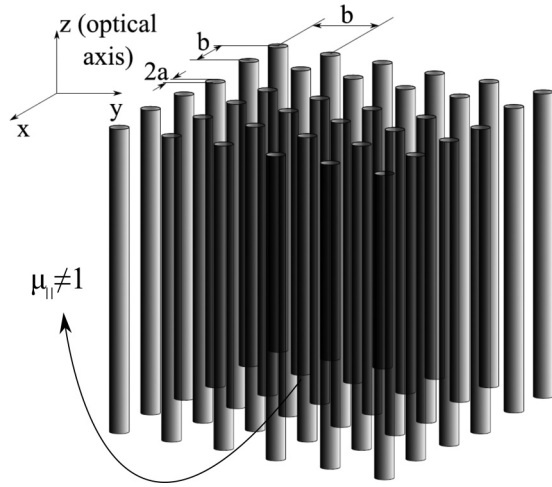


FIG. 1. A medium of long parallel wires which are set in a square lattice. The wires are made of materials whose relative dielectric constant is much larger than unity ( $\epsilon_r \gg 1$ ). Here,  $a$  and  $b$  are the wires radius and lattice constant, respectively. For simplicity, the host medium is free space.

transition is related to the resonant enhancement of radiation of a subwavelength dipole located inside the medium. It is an expected effect which is similar to that studied in Ref. [6]. However, in the present case it holds for a magnetic dipole oriented transversely to nanowires. The sharp dependence of the permeability on the wave vector results in the unusual property of our wire medium—the radiation of the internal magnetic dipole is concentrated at the line which passes through the dipole center parallel to the optical axis. This property is also detectable from the dispersion contours (sections of the dispersion surfaces) of the TE waves. We show these dispersion contours in the region of topological transition and fully concentrate on two effects: the pattern of the internal source and its Purcell factor.

The paper is organized as follows: In Sec. II, we obtain analytical expressions for the magnetic polarizability of a high-index dielectric cylinder and the effective permeability of the corresponding wire medium. In Sec. III, we discuss the implications of the resonant and nonlocal behavior of this permeability and show the simulated results for the radiation of an embedded magnetic dipole. In Sec. IV, we present a brief summary of the work.

## II. EFFECTIVE PERMEABILITY OF THE WIRE MEDIUM

Let a plane wave with electric field polarized along  $y$  axis illuminate a dielectric cylinder, as is shown in Fig. 2. The incident wave has perpendicular polarization, and its magnetic field along  $z$  axis can be written as

$$H_{z_{\text{inc}}} = H_0 e^{-j(k_x x + k_z z)}, \quad (2)$$

where  $H_0$  is the magnitude, and  $k_z$  and  $k_x$  are the wave vector components in the free space. Due to the cylindrical geometry, it is proper to expand the field into cylindrical harmonics.

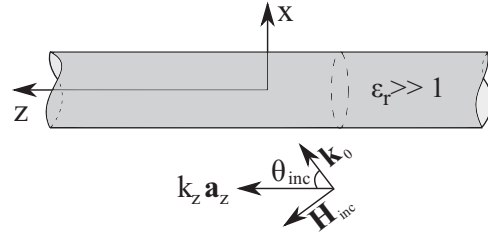


FIG. 2. An infinite dielectric cylinder illuminated by a TE-polarized plane wave.

Therefore,

$$H_{z_{\text{inc}}} = H_0 \sum_m [(-j)^m J_m(h_0 R) e^{jm\phi}] e^{-jk_z z}, \quad (3)$$

in which  $J_m(x)$  is the Bessel function (first kind, order  $m$ ),  $h_0 = \sqrt{k_0^2 - k_z^2}$  ( $k_0$  is the free-space wave number) and  $(R, \phi, z)$  are the components of the cylindrical coordinate system.

Taking into account the scattering and penetration of the wave into the dielectric cylinder, the total electromagnetic fields outside and inside the cylinder can be described by

$$\begin{aligned} E_{z_{\text{out}}} &= \sum_m [C_m H_m^{(2)}(h_0 R) e^{jm\phi}] e^{-jk_z z}, \\ H_{z_{\text{out}}} &= \sum_m [(D_m H_m^{(2)}(h_0 R) + H_0 (-j)^m J_m(h_0 R)) e^{jm\phi}] e^{-jk_z z}, \end{aligned} \quad (4)$$

and

$$\begin{aligned} E_{z_{\text{in}}} &= \sum_m [A_m J_m(hR) e^{jm\phi}] e^{-jk_z z}, \\ H_{z_{\text{in}}} &= \sum_m [B_m J_m(hR) e^{jm\phi}] e^{-jk_z z}, \end{aligned} \quad (5)$$

where  $h = \sqrt{k_0^2 \epsilon_r - k_z^2}$  ( $\epsilon_r$  denotes the relative dielectric constant of the cylinder) and  $H_m^{(2)}(x)$  represents the Hankel function (second kind, order  $m$ ). The other components of the electromagnetic fields ( $E_R$ ,  $H_R$ ,  $E_\phi$ , and  $H_\phi$ ) can be readily derived by solving the Maxwell's equations. Therefore,

$$\begin{aligned} E_R &= \frac{1}{h^2} \left( -jk_z \frac{\partial E_z}{\partial R} - \frac{j\omega\mu_0}{R} \frac{\partial H_z}{\partial \phi} \right), \\ E_\phi &= \frac{1}{h^2} \left( \frac{-jk_z}{R} \frac{\partial E_z}{\partial \phi} + j\omega\mu_0 \frac{\partial H_z}{\partial R} \right), \\ H_R &= \frac{1}{h^2} \left( \frac{j\omega\epsilon}{R} \frac{\partial E_z}{\partial \phi} - jk_z \frac{\partial H_z}{\partial R} \right), \\ H_\phi &= \frac{1}{h^2} \left( -j\omega\epsilon \frac{\partial E_z}{\partial R} - \frac{jk_z}{R} \frac{\partial H_z}{\partial \phi} \right). \end{aligned} \quad (6)$$

The above equation [Eq. (6)] indicates that the waves inside and outside the cylinder are hybrid. In Eqs. (4) and (5), the unknown coefficients ( $A_m$ ,  $B_m$ ,  $C_m$ , and  $D_m$ ) are related to each other through boundary conditions, i.e., the tangential components of the electric and magnetic fields should be continuous at the radius of the cylinder ( $R = a$ ). After determining the fields inside the cylinder, we can obtain the polarization current that is equal to  $\mathbf{J}_p = j\omega\epsilon_0(\epsilon_r - 1)\mathbf{E}_{\text{in}}$ . On

the other hand, we know that the magnetic moment per unit length of our cylinder is described by

$$\mathbf{m} = \frac{1}{2} \mu_0 \int_S \mathbf{r} \times \mathbf{J}_p dS, \quad (7)$$

where  $\mathbf{r} = \mathbf{R} + z\mathbf{a}_z$  is the distance vector from the origin to the current element. Therefore, the  $z$  component of the magnetic moment can be obtained as

$$m_z = \frac{1}{2} j\omega\mu_0\epsilon_0(\epsilon_r - 1) \int_S R^2 E_{\phi_{in}} dR d\phi, \quad (8)$$

in which the  $\phi$  component of the electric field inside the cylinder is as follows:

$$E_{\phi_{in}} = \frac{j\omega\mu_0}{h} \sum_m \left[ \left( A_m \frac{mk_z}{j\omega\mu_0 h R} J_m(hR) + B_m J'_m(hR) \right) e^{jm\phi} \right] e^{-jk_z z}. \quad (9)$$

The function  $J'_m(x)$  is the derivative of  $J_m(x)$ . From the Eqs. (8) and (9), we can see that the only cylindrical harmonic which is responsible for nonzero magnetic moment per unit length produced by the magnetic field of the incident wave is  $m = 0$ . Then, based on Eq. (9), we should only calculate the coefficient  $B_0$ — $A_0$  gives the zero contribution into Eq. (8). From imposing the boundary conditions to determine the unknown coefficients, we can achieve

$$B_0 = \frac{j2h}{\pi h_0 a [h_0 J'_0(ha) H_0^{(2)}(h_0 a) - h J_0(ha) H_0^{(2)}(h_0 a)]} H_0. \quad (10)$$

If we substitute Eq. (10) into Eq. (9) and use Eq. (8), finally, we derive the magnetic polarizability as

$$\alpha_{mm}^{zz} = \frac{m_z}{\mu_0 H_0} = \frac{j2k_0^2(\epsilon_r - 1)}{h_0(k_0^2\epsilon_r - k_z^2)} \times \frac{[haJ_0(ha) - 2J_1(ha)]}{[h_0J_1(ha)H_0^{(2)}(h_0a) - hJ_0(ha)H_1^{(2)}(h_0a)]}. \quad (11)$$

Notice that we do not use any approximation to derive the magnetic polarizability. To keep only the term with  $m = 0$  in Eq. (9) is the same as to excite our cylinder by only a magnetic field of the electromagnetic wave letting the external electric field be zero at the cylinder axis. Adding a corresponding term to Eq. (2), it is easy to see that the excitation of the cylinder by two plane waves incident on it from two opposite sides and forming the standing wave with the node of the electric field at the  $z$  axis results in the same formula (11). It is worth noting that retaining the term  $A_1$  in Eq. (9), we would attribute to the magnetic moment per unit length the dependence on the incident electric field, and the response of the cylinder would be bianisotropic. Keeping only  $B_0$  we follow the approach of Ref. [21] that allows one to avoid the seeming bianisotropy in the response of a symmetric scatterer. This bianisotropy is not physically sound and would result in inconsistencies of the effective-medium model (see, e.g., in Ref. [22]).

The minus sign in the denominator of the second factor in Eq. (11) allows the resonance of the magnetic polarizability if  $\epsilon_r$  is positive. This is the fundamental Mie resonance of

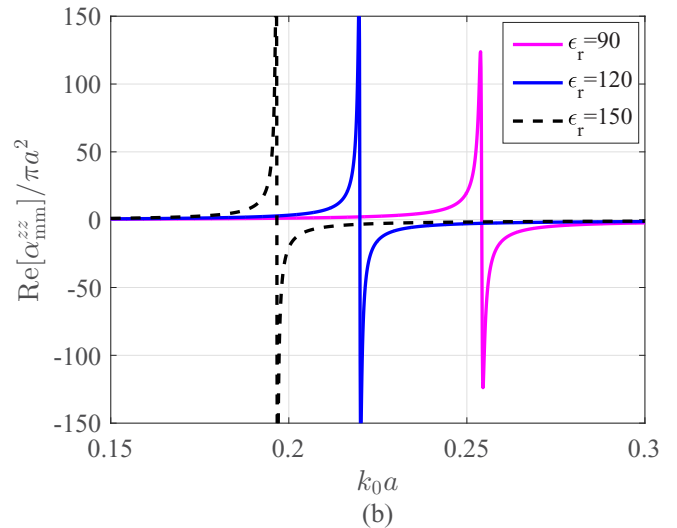
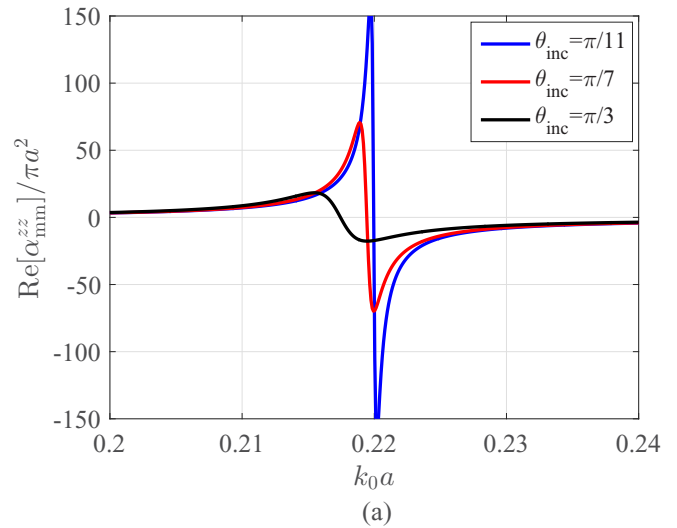


FIG. 3. (a) Real part of the magnetic polarizability versus the normalized frequency for three different incident angles. The relative dielectric constant of the dielectric cylinder is assumed to be  $\epsilon_r = 120$ . (b) Real part of the magnetic polarizability versus the normalized frequency for three different dielectric constants. Here, we assume that  $\theta_{inc} = \pi/11$ .

the cylinder. Since  $k_z$  enters both  $h$  and  $h_0$ , the polarizability is nonlocal, i.e., depends on the angle of incidence  $\theta_{inc}$ . To show the impact of the incidence angle and that of the dielectric constant  $\epsilon_r$  on the Mie resonance, we plot the magnetic polarizability as a function of normalized frequency for several values of  $\epsilon_r$  and  $\theta_{inc}$ . In Fig. 3(a) it is assumed that  $\epsilon_r = 120$ . Then the Mie resonance occurs approximately at  $k_0 a = 0.22$  for all angles. For small angles, the resonance is indeed stronger than that for large angles. Thereby, we see that the resonant polarizability depends strongly on the incident angle or—more specifically—on the axial component  $k_z = k_0 \cos(\theta_{inc})$  of the wave vector.

At frequencies below the Mie resonance band the magnetic polarizability is negligibly small. The location of the resonance on the frequency axis is a function of the dielectric constant of the cylinder, as can be seen in Fig. 3(b). When  $\epsilon_r$  is not

very high, the resonance happens at higher  $k_0a$  and vice versa. For the accuracy of the effective-medium model it is better if the resonance occurs at lower  $k_0a$ . This model requires that both the radius ( $a$ ) and the array period ( $b$ ) of the wires are sufficiently small compared to the wavelength in the host medium, in other words,  $k_0a < k_0b \ll 1$ . Materials such as lithium tantalate, silicon carbide, or hexagonal boron nitride which support phonon polaritons would provide such high dielectric constants at the infrared. The only problem with these materials may be optical losses which are obviously noticeable when  $\varepsilon_r \gg 1$ .

Deriving the effective permeability of the lattice we follow the approach [12,14] which allows us to take into account the nonlocality also in the electromagnetic interaction of cylinders. For the axial component of the effective permeability we have the following formula:

$$\mu_{\parallel} = 1 + \frac{1}{A_{\text{cell}}} \left( \frac{1}{\alpha_{\text{mm}}^{zz}} - C_{\text{int}}^z \right)^{-1}, \quad (12)$$

which is dual to that obtained for the axial permittivity in Ref. [12] with the substitution of the magnetic polarizability by the electric one. Here  $A_{\text{cell}} = b^2$  and  $C_{\text{int}}^z$  is the lattice interaction constant responsible for the dipole-dipole interaction. It is the same for magnetic and electric dipole moment per unit length of the cylinder and was derived in Ref. [12]:

$$C_{\text{int}}^z \approx h_0^2 \left( \frac{j}{4} + \frac{1}{2\pi} \ln \left( \frac{h_0 b}{4\pi} \right) + \xi \right),$$

$$\xi = \frac{C}{2\pi} + \frac{1}{12} + \sum_{n=1}^{\infty} \frac{(e^{2\pi|n|} - 1)^{-1}}{\pi|n|}. \quad (13)$$

Here,  $C$  is the Euler constant. The mutual interaction of the wires is very strong and broadens the collective resonance, therefore the resonance of the effective permeability is not as narrow band as that of the effective magnetic polarizability. Let us choose  $\varepsilon_r = 120$  and the fraction volume  $f_v = \pi a^2/b^2 = 0.1963$  (this corresponds to the relation between the period and the wire radius  $b = 4a$ ). In Fig. 4 we depict the axial component of the effective permeability as a function of  $k_z$  for these design parameters. For very low  $k_0a \ll 0.22$ ,  $\mu_{\parallel}(k_z)$  is approximately uniform and close to unity. The increase of  $k_0a$  results in increasing  $\mu_{\parallel}(k_z)$  especially for the transverse propagation, however it keeps finite and smooth versus  $k_z$ . At frequency  $k_0a = 0.22$ ,  $\mu_{\parallel}(k_z)$  changes its behavior that corresponds to the topological transition. For  $k_0a = 0.2201$  the axial permeability is negative in the interval  $|k_z/k_0| < 0.83$  and becomes positive in  $|k_z/k_0| > 0.83$ . At  $|k_z/k_0| = 0.83$ , there is a vertical asymptote. This resonance of  $\mu_{\parallel}(k_z)$  implies that the transverse component  $q$  of the wave vector experiences a similar resonance at  $|k_z/k_0| = 0.83$ . It is clear from the dispersion equation for TE waves in a magnetic hyperbolic medium [14] (for the case when the host medium is free space  $\varepsilon_h = 1$ ):

$$\frac{q^2}{\mu_{\parallel}(k_z)} + \frac{k_z^2}{\mu_{\perp}} = k_0^2 \varepsilon_{\perp}, \quad (14)$$

in which  $\mu_{\perp} \approx 1$  and  $\varepsilon_{\perp}$  can be found from Ref. [12]. In practical cases—when optical losses are taken into account—the resonance of  $q$  means that  $q$  is a very large imaginary value. As

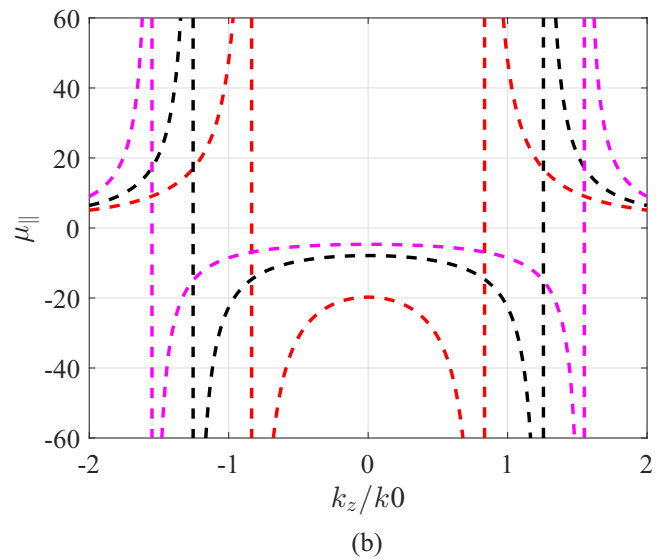
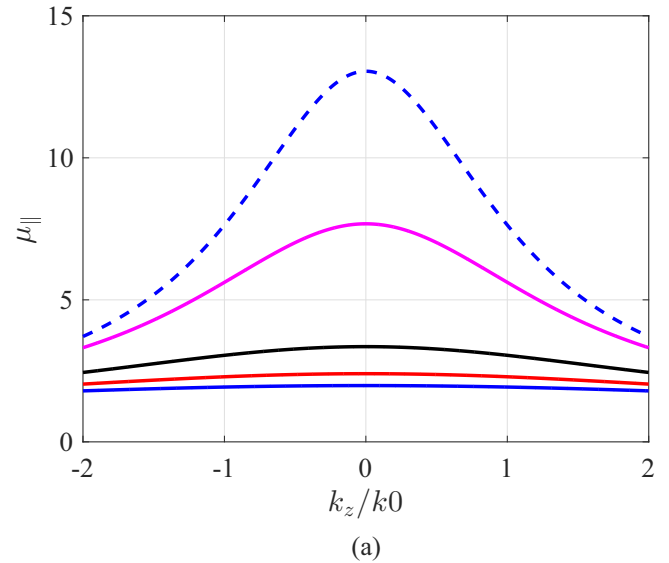


FIG. 4. The parallel component of the effective permeability versus the normalized parallel component of the wave vector, when  $\varepsilon_r = 120$  and  $f_v = 0.1963$ . (a) Frequencies below the topological transition  $k_0a = 0.22$ . Solid blue curve— $k_0a = 0.2058$ , solid red one— $k_0a = 0.2096$ , solid black one— $k_0a = 0.2135$ , solid magenta one— $k_0a = 0.2173$ , and dashed blue one— $k_0a = 0.2182$ . (b) Frequencies above the topological transition  $k_0a = 0.22$ . Dashed red— $k_0a = 0.2201$ , dashed black— $k_0a = 0.2211$ , dashed magenta— $k_0a = 0.2220$ .

we can see in Fig. 4 this effect keeps propagating eigenmodes within a certain range of frequencies. For frequencies  $k_0a \geq 0.23$  the resonances of  $\mu_{\parallel}(k_z)$  still hold but correspond to very high spatial frequencies. For such high spatial frequencies the effective-medium model is not applicable [23]. In our plot in Fig. 4 the region of  $k_z$  (of the order of  $k_0$  or smaller) is compatible with the model.

Imaginary  $q$  for a propagating eigenmode with allowed value of  $k_z$  means that the medium eigenmode propagates along the  $z$  axis, being evanescent in the transverse plane ( $x - y$ ). Very high imaginary  $q$  implies the ultimate subwavelength concentration of the eigenmode in this plane. If we

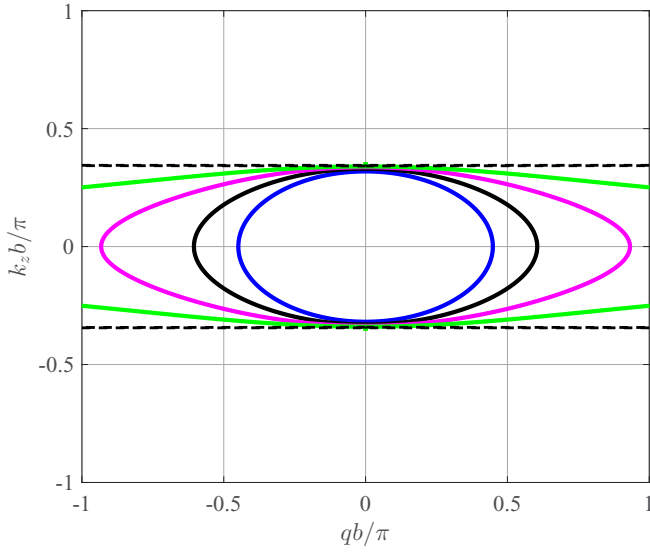


FIG. 5. Dispersion contours of the TE-polarized waves. Here,  $\epsilon_r = 120$  and  $f_v = 0.1963$ . Solid blue curve corresponds to  $k_0 a = 0.2058$ , solid black one— $k_0 a = 0.2135$ , solid magenta one— $k_0 a = 0.2173$ , solid green one— $k_0 a = 0.2194$ , and dashed black one— $k_0 a = 0.2211$ .

embed a subwavelength source of TE waves (such as a point magnetic dipole oriented orthogonally to the  $z$  axis) in our wire medium this mode will be excited, dominating over all other modes propagating along the  $z$  axis. This domination results from the huge slope of the curve  $\mu_{\parallel}(k_z)$  which implies the huge density of electromagnetic states. It can also be seen from the dispersion contours of the TE-polarized waves shown in Figure 5. As Fig. 5 indicates, the dispersion surface is transformed from a closed surface (ellipsoid) into an open surface (approximately a flat line, hyperboloid) at transition frequency (notice that each wave vector components travels normal to the dispersion surface). This feature was noticed for the permittivity tensor of some dielectric hyperbolic metamaterials in Ref. [24]. Our magnetic hyperbolic metamaterial is dual to dielectric hyperbolic metamaterials, and the roles of  $\bar{\epsilon}$  and TM waves are played by  $\bar{\mu}$  and TE waves. Since the dominant mode strongly attenuates in both the  $x$  and  $y$  directions, it means that the whole electromagnetic field generated by our magnetic dipole should be concentrated around the line which passes through the dipole center along the  $z$  axis.

### III. NUMERICAL SIMULATIONS

#### A. Localization of magnetodipole radiation

This filamentary localization of magnetodipole radiation was confirmed by using a 3D electromagnetic simulator CST Microwave Studio. In our simulations we position a strongly subwavelength current loop whose magnetic moment is directed along the  $y$  axis in the center of the wire medium sample as shown in Fig. 6. The medium sample is finite size with length  $L_{\text{sample}} = (N - 1)b + 2a$  where  $N = 12$  is the number of the wires. It has realistic optical losses: We suppose that the tangent of dielectric losses in the material of our wires is equal to  $\tan \delta = 0.1$ , where the complex permittivity

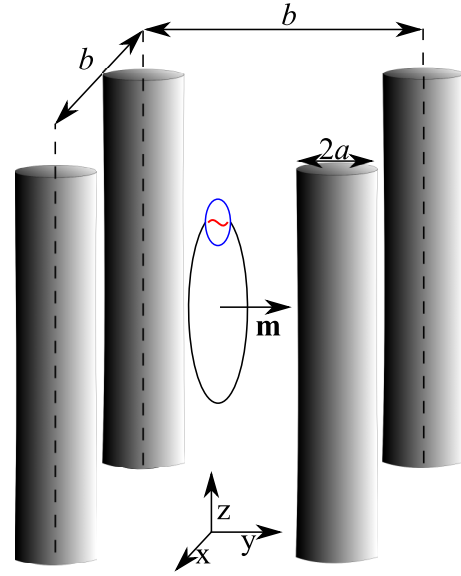


FIG. 6. The subwavelength magnetic dipole oriented perpendicularly to the wire axis and located in the center of the wire medium sample.

of nanowires is  $\epsilon_r = \text{Re}[\epsilon_r][1 - j \tan \delta]$ ,  $\text{Re}[\epsilon_r] = 120$ . This value is the complex permittivity of lithium tantalate at  $f = 23$  THz. The radius of the wires is  $a = 455$  nm and  $b = 4a$  as above. The spatial distribution of the transverse component of the electric field (the  $x$  component in the  $y - z$  plane) is shown in Fig. 7 for four frequencies. We see that only at the frequency  $k_0 a = 0.2192 \approx 0.22$  the field significantly decays

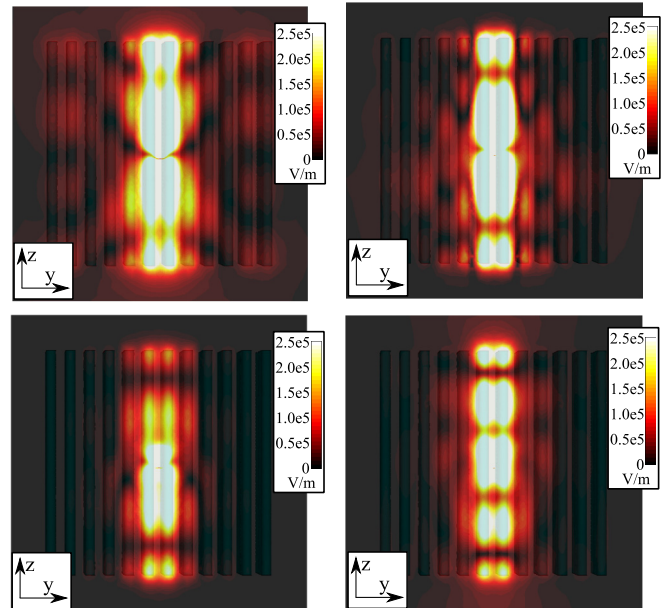


FIG. 7. Distribution of the normal component of the electric field in the wire-medium sample (consisting of  $12 \times 12$  nanowires). The magnetic dipole moment located in the center of the sample is along the  $y$  axis. Here,  $\epsilon_r = 120 - j12$ ,  $f_v = 0.1963$ . (a)  $f = 18$  THz ( $k_0 a = 0.1715$ ); (b)  $f = 21$  THz ( $k_0 a = 0.2001$ ); (c)  $f = 23$  THz ( $k_0 a = 0.2192$ ) and (d)  $f = 27$  THz ( $k_0 a = 0.2573$ ).

in the transverse plane so that it is practically concentrated in one unit cell of the wire medium. This is the maximal possible concentration in a composite material—that restricted only by the granularity of the medium. The excited wave propagates along the  $z$  axis and experiences nearly total internal reflection at the interfaces of the medium sample. Similar pictures correspond to other components of the electromagnetic field. The comparison of different components confirms that the wave is TE polarized. At three other frequencies the waves are also TE polarized, whereas their localization is not filamentary and even the crosslike dipole pattern inherent to usual hyperbolic metamaterials [13] can be guessed in Fig. 7(a).

The reason for the striking difference in the internal dipole patterns for our wire medium and the majority of hyperbolic materials is spatial dispersion. Metal wire media operating at microwaves are also spatially dispersive, and the slope of  $\epsilon_{\parallel}(k_z)$  (see, e.g., in Ref. [11]) at their spatial resonance  $|k_z| = k_0$  is as huge as that of our  $\mu_{\parallel}(k_z)$  at their resonant  $k_z$  in the topological transition frequency range. It is not surprising, therefore, that in microwave wire media the similar filamentary dipole pattern was also observed (see, e.g., in Ref. [25]). However, in what concerns this pattern our infrared magnetic wire medium and microwave wire media differ qualitatively. The first difference is duality: Microwave wire media are dielectric hyperbolic metamaterials and the filamentary pattern in them corresponds to transverse *electric* dipoles. The second difference is the bandwidth effect: Microwave wire media are broadband, and the same dipole pattern is inherent for them at any frequency for which the effective-medium model is applicable. Our wire media possess the dipole pattern which strongly varies versus frequency; this is illustrated by Fig. 7. The filamentary pattern of the magnetic dipole corresponds only to the range of the topological transition.

### B. Purcell factor

Another implication of the topological transition (where the isofrequency of the medium transits from the closed-surface (elliptical) regime to open-surface (hyperbolic) regime) is the strong Purcell effect in our magnetic metamaterial. Originally, the effect was known as the enhancement of the decay rate of a quantum emitter located in an open cavity [26,27]. However, the role of the cavity is only to extract more power from the emitter, whereas the enhancement of its decay rate is the same as the enhancement of the radiated power. Therefore, the notion of the Purcell effect was extended first to any scatterer located in the vicinity of an emitter [28–31] and finally to any active radiator whose radiation is enhanced by any environment different from free space [6,32,33].

Based on this general concept, we can define the magnetic Purcell factor of our wire medium as the increase of the radiated power of a subwavelength magnetic dipole due to the presence of the wire medium around it. According to the “antenna terminology,” the radiated power of the emitter is proportional to the radiation resistance of that emitter [34]. Therefore, to calculate the Purcell factor, it is the same as to obtain the ratio of the radiation resistances in the presence of the wire medium ( $R_r$ ) and in the absence ( $R_0$ ):

$$P_F = \frac{R_r}{R_0}. \quad (15)$$

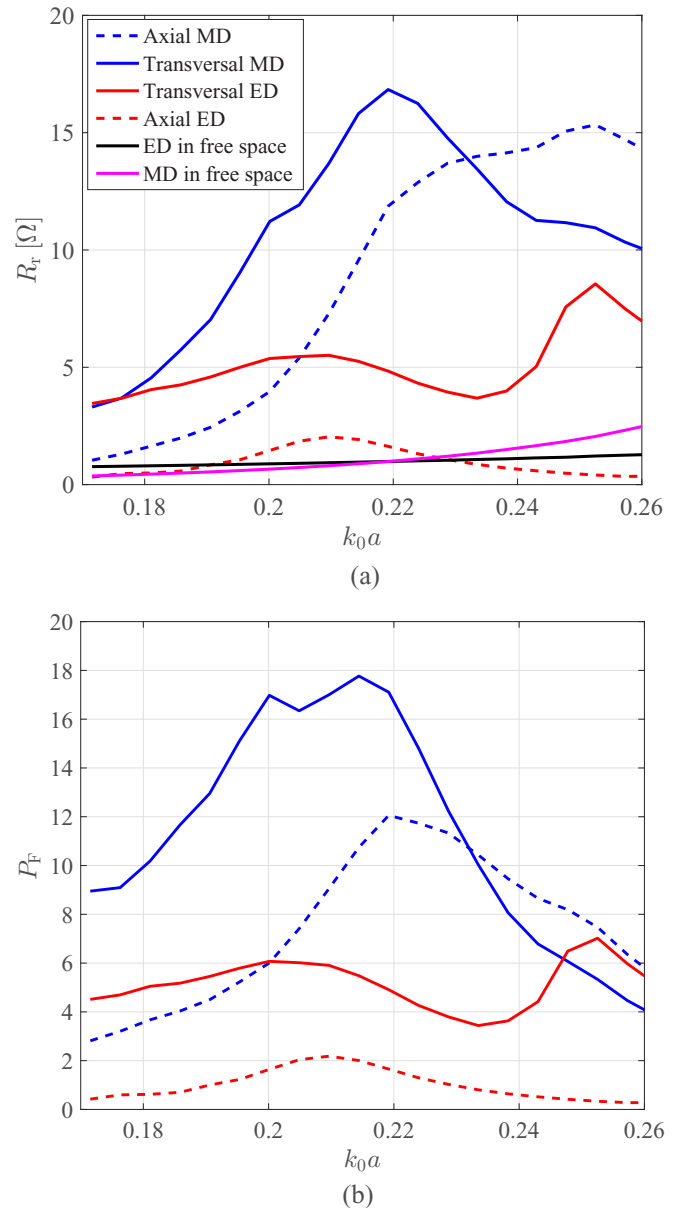


FIG. 8. (a) Radiation resistance of subwavelength magnetic (MD) and electric (ED) dipoles located in the center of the wire-medium sample (including  $12 \times 12$  wires) and the free space. (b) Corresponding Purcell factor. Here,  $\epsilon_r = 120 - j12$  and  $f_v = 0.1963$ .

For the same structure as above we have simulated the radiation resistances. Besides the case of the transverse magnetic dipole shown in Fig. 6, we have studied the case when the same magnetic dipole is oriented in parallel to the  $z$  axis. Also, we simulated the cases of the transverse and axial electric dipoles of the same subwavelength size, all centered at the same point as in Fig. 6. In Fig. 8(a) which depicts the radiation resistance versus frequency, the blue curves refer to the magnetic dipole in the presence of the sample. As one can see, the radiation resistance of the magnetic dipole oriented perpendicularly to the optical axis experiences the strong resonance at  $k_0 a \approx 0.22$ , exactly where the effective-medium model predicts the topological transition. Notice that similar to what we did in our previous works [6,35], in order

to be sure that our effect is not distorted by dimensional resonances, we simulated the metamaterial sample with three different sizes, corresponding to  $10 \times 10$ ,  $12 \times 12$  and  $14 \times 14$  wires, respectively ( $L_{\text{sample}} = 9b + 2a$  for  $N = 10$ ,  $L_{\text{sample}} = 11b + 2a$  for  $N = 12$  and  $L_{\text{sample}} = 13b + 2a$  for  $N = 14$ ). The radiation resistances of these three cases are almost the same and they do not differ especially at the topological transition. This clearly confirms that dimensional resonances do not exist.

In Fig. 8(a), the dashed blue curve shows weaker effect for the parallel magnetic dipole. Red solid and dashed curves correspond to the perpendicular and parallel electric dipoles, respectively. For comparison with the case when the host is free space, the frequency dispersion of  $R_0$  is given in the same plot for both electric and magnetic dipoles. Figure 8(b) presents the frequency dispersion of the Purcell factor for all four dipoles. It is clearly seen that the strongest resonance and highest  $P_F$  correspond to the transversal magnetic dipole. An axial magnetic dipole also experiences the resonance at the topological transition. However, the resonant values of  $P_F$  are smaller because this magnetic dipole mainly creates the TE-polarized radiation which weakly interacts with the nanowires. Therefore, it is not enhanced.

The values of  $P_F$  for the axial electric dipole are low. It is not surprising. Recall that in a wire medium of perfectly conducting (PC) wires the radiation of the axial electric dipole is fully suppressed [5]. The suppression results from the destructive near-field coupling of the dipole with adjacent wires. The axial current of the dipole induces opposite axial currents in them which cancel the radiation. This effect is similar to the suppression of radiation of a horizontal electric dipole located on the PC substrate. Well, our wires are not PC, they are highly refractive. However, the substrates with high positive permittivity and finite negative permittivity also suppress the radiation of the horizontal electric dipole. This destructive interaction originates from the capacitive coupling causes the inverse mirror image of the horizontal electric dipole in the substrate with the strong skin effect. A similar situation holds for the axial dipole source in wire media if the wires possess strong skin effect. If the wires have high or negative  $\epsilon_r$ , the values of  $P_F$  for the axial electric dipole should be low. However, we can see in Fig. 8(b) that the radiation of this dipole experiences the resonance (at slightly lower frequency than that of the magnetic topological transition). This is also not surprising, because not all radiation of an axial electric dipole is TM polarized. It also produces some TE waves, and this effect is competing with the capacitive destructive interaction. Therefore, we have  $P_F = 2$  at  $k_0 a = 0.21$ , whereas far from this frequency we see  $P_F \approx 0$ . As to the noticeable enhancement of the transverse electric dipole, it, definitely, occurs due to the constructive interaction of this dipole with the adjacent nanowires (similar to a vertical dipole on the

high-permittivity substrate). This effect is complemented by the resonant enhancement of TE-polarized waves. However, in the near zone of the electric dipole the magnetic field is weak. Therefore, an electric dipole cannot interact with the magnetic medium as strongly as a magnetic dipole, and the resonant Purcell factor of the transversal magnetic dipole is higher.

As mentioned before, we position the transversal magnetic dipole source symmetrically with respect to the surrounding wires. However, our simulated results show that the Purcell factor is sensitive to the position of the source within the unit cell shown in Fig. 6. They indicate that if the transversal magnetic dipole is shifted along the diagonal of the unit cell, the Purcell factor significantly increases. This is similar to the case of the transversal electric dipole located in a wire medium of perfectly conducting (PC) wires [5].

#### IV. CONCLUSIONS

In this paper we calculated the effective permeability of a simple wire medium whose wires are made of a material with high positive dielectric constant. Its parallel component  $\mu_{\parallel}$  is resonant due to the Mie resonance of a single wire and is an indefinite function of both frequency and axial wave vector  $k_z$  (changes the sign depending on these arguments). This change of the sign results in a transition in the topology of the dispersion surface for TE polarized waves. In the frequency range of the topological transition, the huge (filamentary) localization of radiation occurs for an internal magnetic source that clearly shares our medium out from other hyperbolic metamaterials, including that introduced in Ref. [14]. Though a similar pattern is inherent to the medium of perfectly conducting wires operating at microwaves, in our case this pattern corresponds to the magnetic dipole and occurs only at the topological transition.

Our wire medium manifests a strong radiation enhancement for an internal dipole source. Unlike dielectric hyperbolic metamaterials, including microwave wire media, and polaritonic media operating at higher frequencies [6], the maximal enhancement corresponds to magnetic dipoles. Unlike spiral media [14] it holds at the topological transition and the maximal radiation enhancement corresponds to the transversal magnetic dipole.

From the comparison of the present paper with Ref. [6] it is clear that the same polaritonic wire media which manifest the resonant effects related to the regime *epsilon-near-zero* at 35–45 THz [6] may manifest the similar (but different) resonant effects related to the regime *mu-near-zero* in the range 15–30 THz. This is another argument in favor of this type of hyperbolic metamaterials, which definitely deserve more attention from theorists and an experimental implementation to confirm the claimed effects.

[1] A. V. Kabashin, P. Evans, S. Pastkovsky, W. Hendren, G. A. Wurtz, R. Atkinson, R. Pollard, V. A. Podolskiy, and A. V. Zayats, Plasmonic nanorod metamaterials for biosensing, *Nat. Mater.* **8**, 867 (2009).

[2] Y. Zhao, G. Palikaras, P. A. Belov, R. F. Dubrovka, C. R. Simovski, Y. Hao, and C. G. Parini, Magnification of subwavelength field distributions using a tapered array of metallic wires with planar interfaces and an embedded

- dielectric phase compensator, *New J. Phys.* **12**, 103045 (2010).
- [3] B. D. F. Casse, W. T. Lu, Y. J. Huang, E. Gultepe, L. Menon, and S. Sridhar, Super-resolution imaging using a three-dimensional metamaterials nanolens, *Appl. Phys. Lett.* **96**, 023114 (2010).
- [4] Z.-K. Zhou, M. Li, Z.-J. Yang, X.-N. Peng, X.-R. Su, Z.-S. Zhang, J.-B. Li, N.-C. Kim, X.-F. Yu, L. Zhou, Z.-H. Hao, and Q.-Q. Wang, Plasmon-mediated radiative energy transfer across a silver nanowire array via resonant transmission and subwavelength imaging, *ACS Nano* **4**, 5003 (2010).
- [5] A. N. Poddubny, P. A. Belov, and Y. S. Kivshar, Purcell effect in wire metamaterials, *Phys. Rev. B* **87**, 035136 (2013).
- [6] M. S. Mirmoosa, S. Yu. Kosulnikov, and C. R. Simovski, Unbounded spatial spectrum of propagating waves in a polaritonic wire medium, *Phys. Rev. B* **92**, 075139 (2015).
- [7] C. Simovski, S. Maslovski, I. Nefedov, S. Kosulnikov, P. Belov, and S. Tretyakov, Hyperlens makes thermal emission strongly super-Planckian, *Photon. Nanostruct. Fundam. Appl.* **13**, 31 (2015).
- [8] I. S. Nefedov, and C. R. Simovski, Giant radiation heat transfer through micron gaps, *Phys. Rev. B* **84**, 195459 (2011).
- [9] M. S. Mirmoosa, F. Rütting, I. S. Nefedov, and C. R. Simovski, Effective medium model of wire metamaterials in the problems of radiative heat transfer, *J. Appl. Phys.* **115**, 234905 (2014).
- [10] M. S. Mirmoosa and C. R. Simovski, Micron-gap thermophotovoltaic systems enhanced by nanowires, *Photon. Nanostruct. Fundam. Appl.* **13**, 20 (2015).
- [11] C. R. Simovski, P. A. Belov, A. V. Atrashchenko, and Y. S. Kivshar, Wire metamaterials: Physics and applications, *Adv. Mater.* **24**, 4229 (2012).
- [12] M. G. Silveirinha, Nonlocal homogenization model for a periodic array of  $\epsilon$ -negative rods, *Phys. Rev. E* **73**, 046612 (2006).
- [13] A. Poddubny, I. Irosh, P. Belov, and Y. Kivshar, Hyperbolic metamaterials, *Nat. Photon.* **7**, 948 (2013).
- [14] T. A. Morgado, J. T. Costa, and M. G. Silveirinha, Magnetic uniaxial wire medium, *Phys. Rev. B* **93**, 075102 (2016).
- [15] C. R. Simovski, in *Advances in Electromagnetics of Complex Media and Metamaterials*, edited by S. Zouhdi, A. Sihvola, and M. Arsalane (Kluwer Academic Publishers, Dordrecht, The Netherlands, 2002), pp. 229–244.
- [16] P. A. Belov, C. R. Simovski, and S. A. Tretyakov, Example of bi-anisotropic electro-magnetic crystals: the spiral medium, *Phys. Rev. E* **67**, 056622 (2003).
- [17] S. S. Kruk, Z. J. Wong, E. Pshenay-Severin, K. O'Brien, D. N. Neshev, Y. S. Kivshar, and X. Zhang, Magnetic hyperbolic optical metamaterials, *Nat. Commun.* **7**, 11329 (2016).
- [18] M. Kafesaki, A. A. Basharin, E. N. Economou, and C. M. Soukoulis, THz metamaterials made of phonon-polariton materials, *Photon. Nanostruct. Fundam. Appl.* **12**, 376 (2014).
- [19] S. Foteinopoulou, M. Kafesaki, E. N. Economou, and C. M. Soukoulis, Two-dimensional polaritonic photonic crystals as terahertz uniaxial metamaterials, *Phys. Rev. B* **84**, 035128 (2011).
- [20] H. N. S. Krishnamoorthy, Z. Jacob, E. Narimanov, I. Kretzschmar, and V. M. Menon, Topological transitions in metamaterials, *Science* **336**, 205 (2012).
- [21] C. A. Grimes and D. M. Grimes, Permeability and permittivity spectra of granular materials, *Phys. Rev. B* **43**, 10780 (1991).
- [22] A. Alù, Restoring the physical meaning of metamaterial constitutive parameters, *Phys. Rev. B* **83**, 081102(R) (2011).
- [23] O. Kidwai, S. V. Zhukovsky, and J. E. Sipe, Dipole radiation near hyperbolic metamaterials: Applicability of effective-medium approximation, *Opt. Lett.* **36**, 2530 (2011).
- [24] Z. Jacob, J. Y. Kim, G. V. Naik, A. Boltasseva, E. E. Narimanov, and V. M. Shalaev, Engineering photonic density of states using metamaterials, *Appl. Phys. B* **100**, 215 (2010).
- [25] I. S. Nefedov and A. J. Viitanen, Effective medium approach for subwavelength resolution, *Electron. Lett.* **43**, 1206 (2007).
- [26] E. M. Purcell, Spontaneous emission probabilities at radio frequencies, *Phys. Rev.* **69**, 674 (1946).
- [27] L. Novotny and B. Hecht, *Principles of Nano-Optics* (Cambridge University Press, Cambridge, UK, 2006).
- [28] C. Sauvan, J. P. Hugonin, I. S. Maksymov, and P. Lalanne, Theory of the Spontaneous Optical Emission of Nanosize Photonic and Plasmon Resonators, *Phys. Rev. Lett.* **110**, 237401 (2013).
- [29] M. Pelton, Modified spontaneous emission in nanophotonic structures, *Nat. Photon.* **9**, 427 (2015).
- [30] F. Tam, G. P. Goodrich, B. R. Johnson, and N. J. Halas, Plasmonic enhancement of molecular fluorescence, *Nano Lett.* **7**, 496 (2007).
- [31] P. Anger, P. Bharadwaj, and L. Novotny, Enhancement and Quenching of Single-Molecule Fluorescence, *Phys. Rev. Lett.* **96**, 113002 (2006).
- [32] Z. Jacob, I. I. Smolyaninov, and E. E. Narimanov, Broadband Purcell effect: Radiative decay engineering with metamaterials, *Appl. Phys. Lett.* **100**, 181105 (2012).
- [33] A. E. Krasnok, A. P. Slobozhanyuk, C. R. Simovski, S. A. Tretyakov, A. N. Poddubny, A.E. Miroschnichenko, Y. S. Kivshar, and P. A. Belov, An antenna model for the Purcell effect, *Sci. Rep.* **5**, 12956 (2015).
- [34] C. A. Balanis, *Antenna Theory, Analysis and Design* (John Wiley & Sons, New Jersey, 2005).
- [35] M. S. Mirmoosa, S. Yu. Kosulnikov, and C. R. Simovski, Double resonant wideband Purcell effect in wire metamaterials, *J. Opt.* **18**, 095101 (2016).